Controlled Synthesis of Organic Two-dimensional Nanostructures via Reaction-driven, Cooperative Supramolecular Polymerization

Shikha Dhiman,[‡a] Rita Ghosh,[‡ab] Souvik Sarkar [a] and Subi J. George [a]*

Table of Contents

1. General Methods

NMR Measurements: NMR spectra were recorded with a Bruker AVANCE 400 (400 MHz) Fourier transform NMR spectrometer with chemical shifts reported in parts per million (ppm) with respect to TMS.

Optical Measurements: UV-Visible absorption spectra were recorded on a Perkin Elmer Lambda 900 UV-Vis-NIR Spectrometer and emission spectra were recorded on Perkin Elmer LS 55 Luminescence Spectrometer. Path length of 10 mm was used otherwise it is mentioned. Fluorescence spectra of solutions were recorded with 320 nm excitation wavelength. 10 mm x 10 mm or 10 mm x 2 mm quartz cuvettes were used for measurements. The kinetics are started from zero to elucidate the growth kinetics and dormant state CT contributions are avoided. Hence, a change in absorption is monitored.

Transmission Electron Microscopy (TEM): TEM measurements were performed on JEOL JEM 3010 operated at 300 kV. Samples were prepared by placing a drop of solution on carbon coated copper grids followed by drying at room temperature. The images were recorded with an operating voltage of 300 kV. In order to get a better contrast, the samples were stained with uranyl acetate (0.1 wt % in water) before the measurements.

Atomic Force Microscopy (AFM): AFM measurements were performed on a Veeco di Innova SPM operating in tapping mode regime. Micro-fabricated silicon cantilever tips doped with phosphorus with frequency between 235 and 278 kHz and a spring constant of 20-40 Nm^{-1} were used. The samples were prepared by drop casting the solution on silicon substrate and dried in air followed by vacuum drying at room temperature.

Dynamic Light Scattering experiments (DLS): The measurements were carried out using a NanoZS (Malvern UK) employing a 532 nm laser at a back scattering angle of 173°.

Confocal microscopy: Confocal microscopy imaging was done at room temperature using a Zeiss LSM 510 META laser scanning confocal microscope with a laser excitation of λ_{exc} = 560 nm. The microscope objective of 63X (NA 1.4) and 100X (NA 0.5) were employed.

2. Experimental Procedures

Synthesis of MVCHO: The synthesis was done by following the previous report.[S1]

Procedure for kinetically controlled growth: Solution of [**PN**] = [**MVCHO**] = 5×10^{-4} M at pH 11.5 is made. To it required eq. of **8A** were added and kinetics were monitored.

Procedure for kinetically controlled growth with Nile red dye for confocal microscopy imaging: Solution of [**PN**] = [**MVCHO**] = 5×10^{-4} M and 1 μM Nile red dye at pH 11.5 is prepared. To it required eq. of **8A** were added and kinetics were monitored.

3. Packing parameter calculation

The packing factor (*f*) [S2] was calculated using the following equations.

Tanford equations:

$\boldsymbol{l} = 1.5 + 1.265\,\boldsymbol{n}$ (S1)

$\boldsymbol{v} = 27.4 + 26.9\,\boldsymbol{n}$ (S2)

For CS-MVCHO-8A:

$\boldsymbol{n}$ = 8, $\boldsymbol{d}$ = 5.4 Å

$\boldsymbol{l} = 1.5 + 1.265\,(\mathbf{8}) = 11.62$ (S1)

$\boldsymbol{v} = 27.4 + 26.9\,(\mathbf{8})$ = 242.6 (S2)

$\boldsymbol{a} = \pi\left(\frac{\boldsymbol{d}}{2}\right)^2 = \pi\left(\frac{7.5}{2}\right)^2$ = 44.15 (S3)

$\boldsymbol{f} = \frac{\boldsymbol{v}}{\boldsymbol{al}} = \frac{\mathbf{242.6}}{\mathbf{44.15\times11.62}}$ = 0.47 (S4)

For PN-MVCHO-8A:

$\boldsymbol{n}$ = 8, $\boldsymbol{d}$ = 5.4 Å

$\boldsymbol{l} = 1.5 + 1.265\,(\mathbf{8}) = 11.62$ (S1)

$\boldsymbol{v} = 27.4 + 26.9\,(\mathbf{8})$ = 242.6 (S2)

$\boldsymbol{a} = \pi\left(\frac{\boldsymbol{d}}{2}\right)^2 = \pi\left(\frac{5.4}{2}\right)^2$ = 22.89 (S3)

$\boldsymbol{f} = \frac{\boldsymbol{v}}{\boldsymbol{al}} = \frac{\mathbf{242.6}}{\mathbf{22.89\times11.62}}$ = 0.91 (S4)

4. PDI calculation

Length, width and area analysis of the confocal microscopy images was done using LSM image examiner. A frequency statistics was done on the obtained length, width, area and aspect ratio.

$An = \frac{\sum_{i=1}^{n} NiAi}{\sum_{i=1}^{n} Ni}$ $Aw = \frac{\sum_{i=1}^{n} NiAi^2}{\sum_{i=1}^{n} NiAi}$ $PDI = \frac{Aw}{An}$ (S5)

Aspect ratio = $\frac{Length}{Width}$

An = number average sheet area

Aw = weight average sheet area

PDI = polydispersity index

Ai = mean length of size *i*

Ni is the frequency of area *Ai*

Triplicate samples were prepared and visualized though confocal microscopy to capture 2D sheet assembly and calculate their length and width. The corresponding areas in μm^2 by multiplying length and width and aspect ratio by dividing length with width were accounted for statistical analysis.

5. Supporting Figures

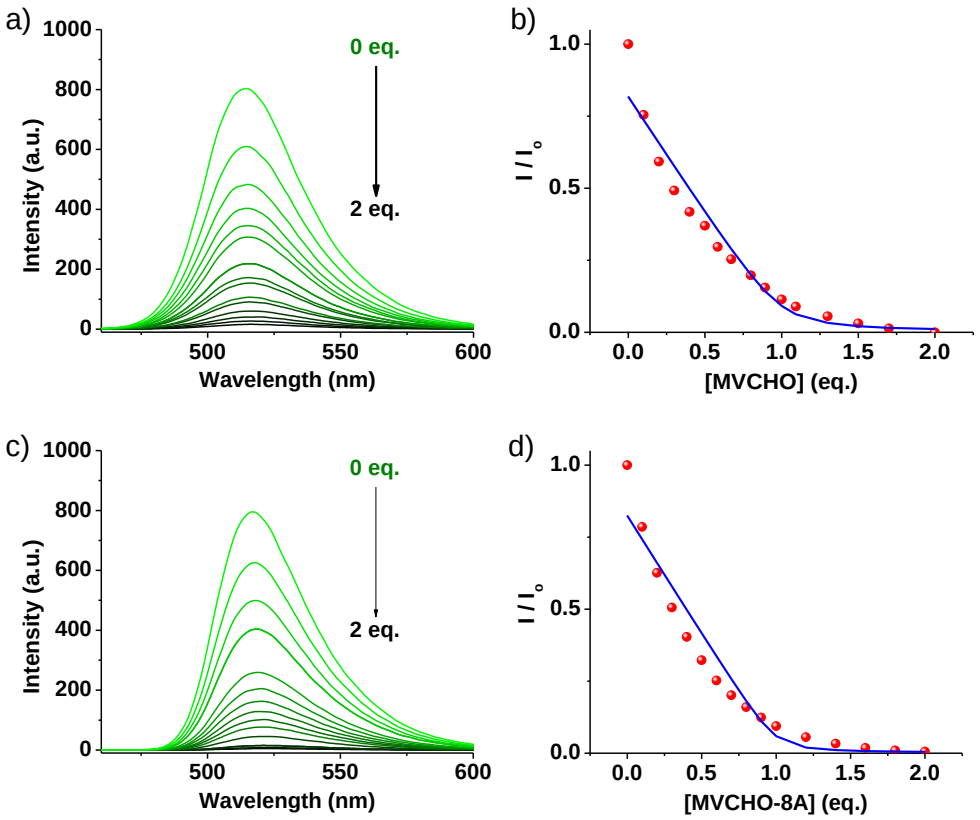

Figure S1. Emission spectra of **PN** on titration with a) **MVCHO** and c) **MVCHO-8A**. Corresponding equivalent vs. emission intensity at 510 nm along with their nonlinear least-square fitting of 1:1 binding model for b) **MVCHO** and d) **MVCHO-8A**. [**PN**] = [**MVCHO**] = [**8A**] = 5x10^{-4} M, pH = 11.5. (λ_{ex} = 350 nm)

Note: Association constant (K_a) was calculated by fitting their titration using following equation

$$\Delta F_{obs} = k_{\Delta HG} \frac{\left(H_0 + G + \frac{1}{K_a}\right) + \sqrt{(H_0 + G_0 + \frac{1}{K_a})^2 - 4H_0G_0}}{2} \qquad \text{(S6)}$$

ΔF is the fluorescence changes at 510 nm,
H_0 = [**PN**] = 5x10^{-3} M,
G_0 = [**MVCHO**] or [**MVCHO-8A**] = 5x10^{-3} M,
K_a is the binding constant between donor and acceptor
$k_{\Delta HG}$ = response factor

It is assumed that the fluorescence change is in a linear relationship with the concentration of donor-acceptor complex in the solution. The fluorescence titration is fitted to equation (S6) using nonlinear least-squares curve-fitting method.

The binding constant (K_a) between the **PN** and **MVCHO** was calculated to be 1.7x10^5 M^{-1} and the binding constant (K_a) between the **PN** and **MVCHO-8A** was calculated to be 3.6x10^5 M^{-1}.

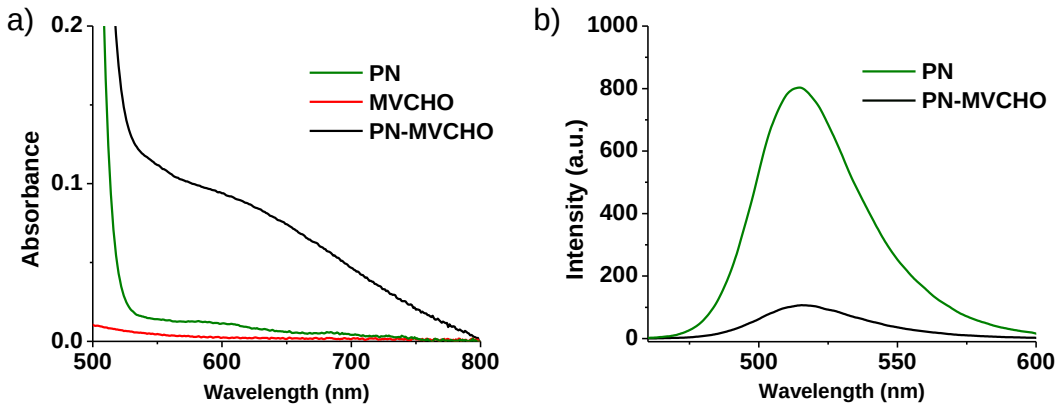

Figure S2. a) Absorption and b) emission spectra of **PN** (donor), **MVCHO** (acceptor) and CT-complex (**PN-MVCHO**, 1:1) [**PN**] = [**MVCHO**] = [**8A**] = 5×10^{-4} M, pH = 11.5. (λ_{ex} = 350 nm)

Note: a) Absorption spectra shows appearance of a new CT band. b) Emission spectra depicts quenching of **PN** emission after CT formation.

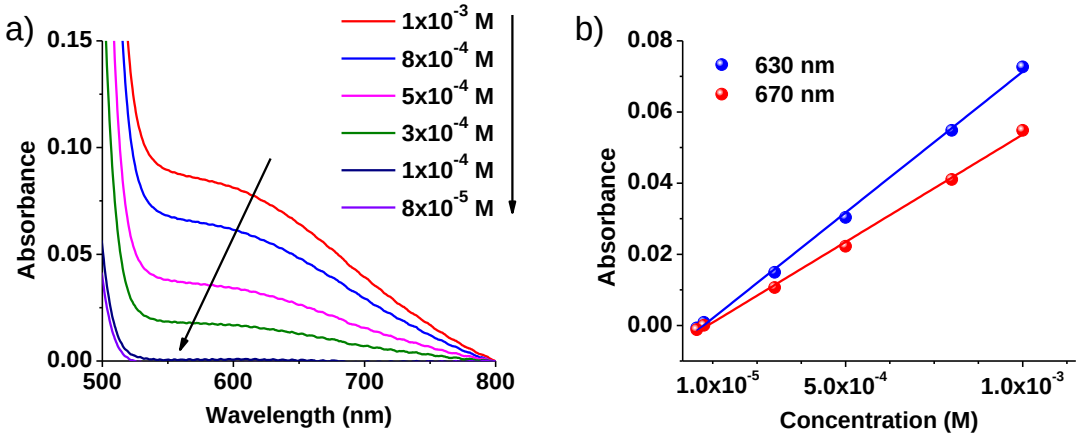

Figure S3. Concentration dependent a) Absorption spectra and b) Absorption changes at 630 and 670 nm of CT-complex (**PN-MVCHO**, 1:1). pH = 11.5. (path length = 5 mm)

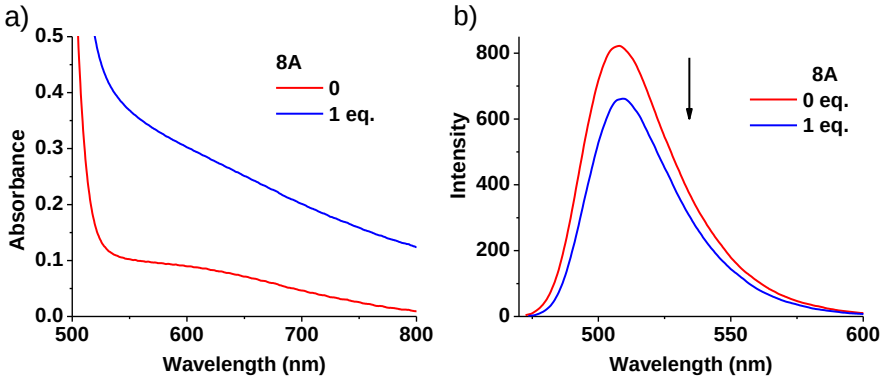

Figure S4. Absorption and emission spectra of **PN-MVCHO** (dormant monomer) and **PN-MVCHO-8A** self-assembly. a) Absorption spectra showing an enhanced CT band on self-assembly. b) Emission spectra depicting quenching of **PN** emission after self-assembly due to increased CT strength. [**PN**] = [**MVCHO**] = [**8A**] = 5×10^{-4} M, pH = 11.5. (λ_{ex} = 350 nm)

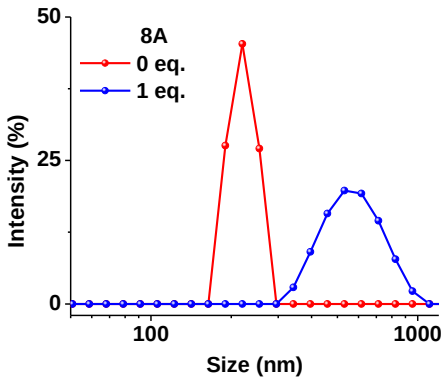

Figure S5. DLS intensity % size measurement of **PN-MVCHO** (dormant monomer) and **PN-MVCHO-8A** self-assembly confirming the formation of supramolecular assembly. [**PN**] = [**MVCHO**] = [**8A**] = $5x10^{-4}$ M, pH = 11.5

Note: Dynamic light scattering (DLS) measurement showed an increase in size for **PN-MVCHO-8A** suggesting the formation of imine-reaction driven formation of CT-amphiphile and further aggregation. DLS has been only used as qualitative indicator and no quantitative analysis is drawn out of it.

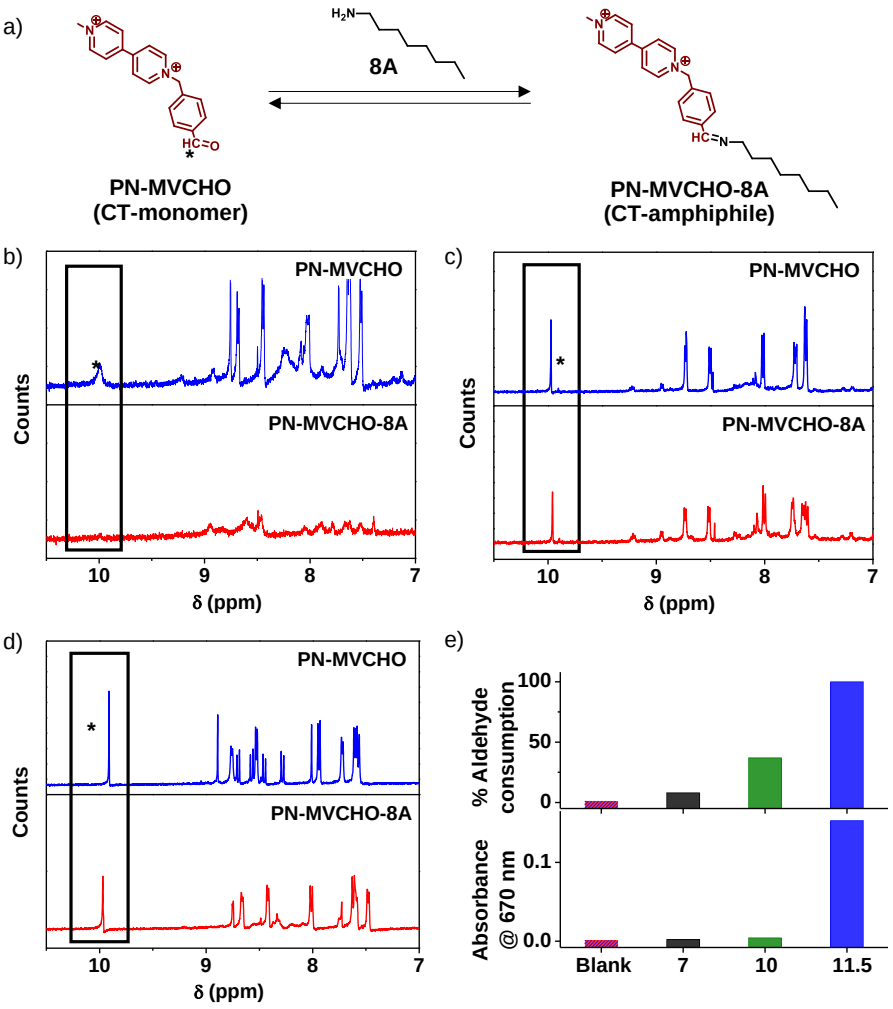

Figure S6. a) Chemical reaction of **MVCHO** with **8A** to result in **MVCHO-8A**, with * representing aldehyde proton. b-d) ^{1}H NMR of **PN-MVCHO** (top) and **PN-MCHO-8A** (bottom) after 2 hours in D_2O at pH 11.5 with sodium acetate as internal standard. b) pH 11.5, c) pH 7 and d) pH 10. e) Comparison of % aldehyde consumption after saturation of growth at different pH. [**PN**] = [**MVCHO**] = [**8A**] = $5x10^{-4}$ M.

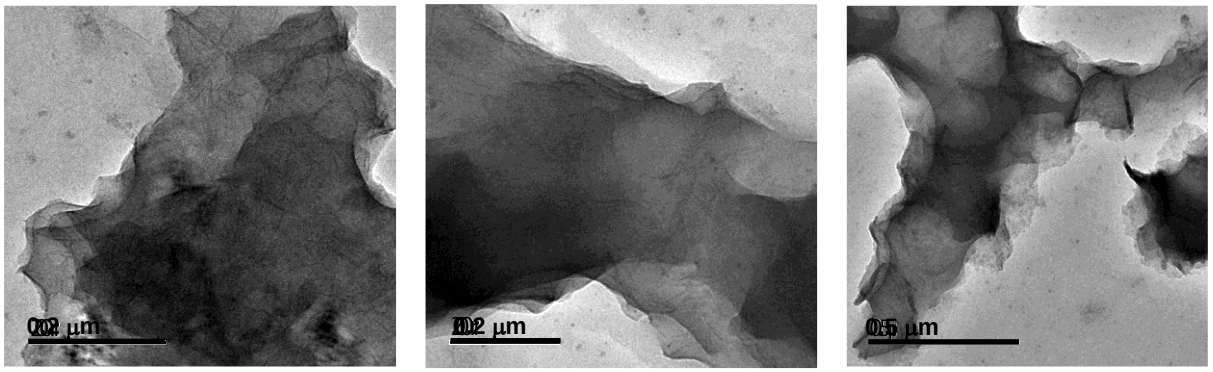

Figure S7. TEM images of **PN-MVCHO-8A** assembly showing the formation of 2D sheets. [**PN**] = [**MVCHO**] = [**8A**] = $5x10^{-4}$ M, pH = 11.5

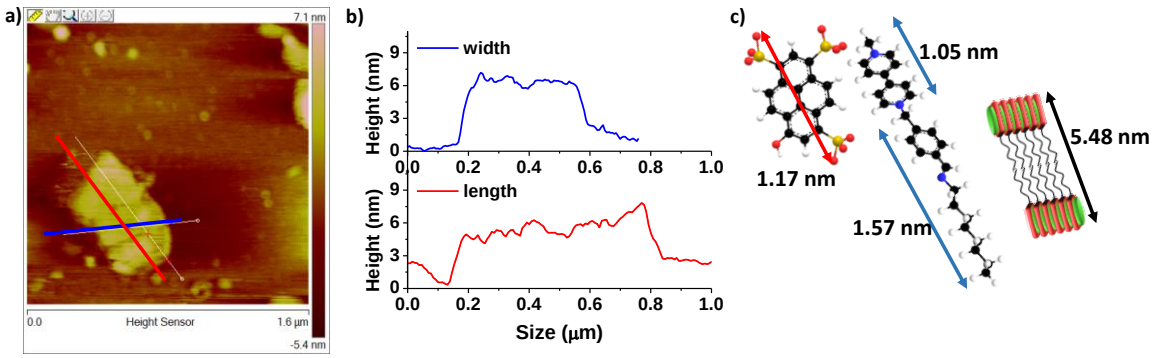

Figure S8. a) Atomic Force Microscopy (AFM) image of **PN-MVCHO-8A** depicting 2D sheet morphology. b) Height profile of the sheets through width and length showing a height of 5.5 nm matching well with calculated bilayer packing with non-interdigitated alkyl chains. c) Molecular lengths of energy minimized structures of **PN** and **MVCHO-8A** obtained from Chem 3D Pro v.10 software and corresponding schematic representation of proposed bilayer packing of **PN-MVCHO-8A** with bilayer width as 5.48 nm. [**PN**] = [**MVCHO**] = [**8A**] = $5x10^{-4}$ M, pH = 11.5

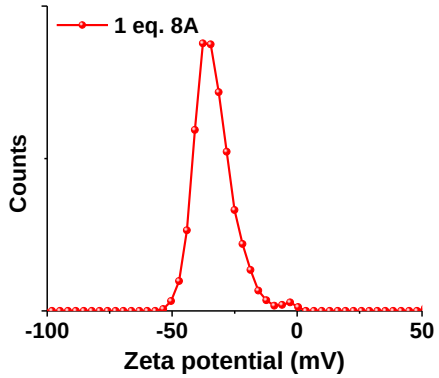

Figure S9. Zeta potential of **PN-MVCHO-8A** depicts negatively charged surface of the sheet. [**PN**] = [**MVCHO**] = [**8A**] = $5x10^{-4}$ M, pH = 11.5

Note: The negatively charged surface will result in repulsive interaction between sheets and hence disfavour the stacking of the sheet at the working concentration.

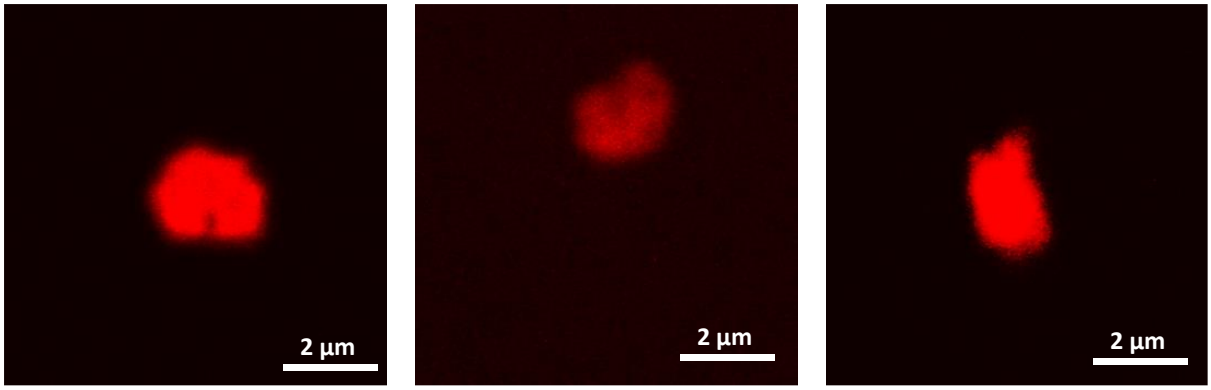

Figure S10. Confocal image (Nile red encapsulated in hydrophobic bilayer) of **PN-MVCHO-8A** assembly showing the formation of 2D sheets. [Nile red] = $1x10^{-6}$ M, [**PN**] = [**MVCHO**] = [**8A**] = 5×10^{-4} M, pH = 11.5.

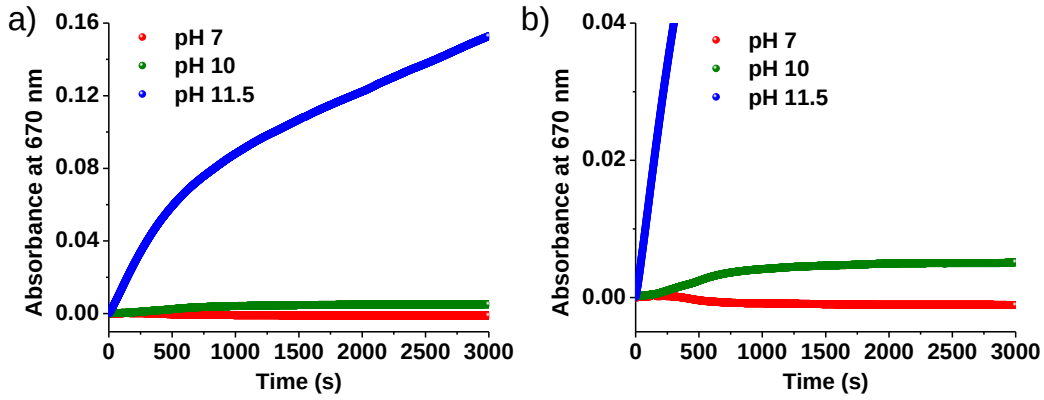

Figure S11. pH-dependence of the imine-driven self-assembly of **PN-MVCHO-8A.** a) Time-dependent absorption changes at 670 nm depicting the dependence of pH to modulate imine reaction kinetics and self-assembly process. b) Corresponding zoomed-in graph to elucidate sigmoidal slow growth at pH 10. [**PN**] = [**MVCHO**] = [**8A**] = 5×10^{-4} M, pH = 11.5.

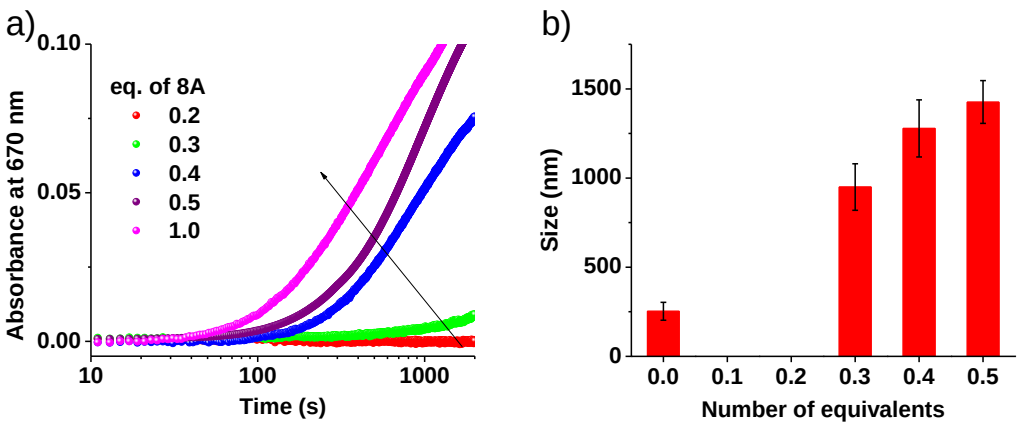

Figure S12. Dependence of amine (**8A**) concentration on the imine-driven self-assembly of **PN-MVCHO-8A.** a) Time-dependent absorption changes at 670 nm with time in log scale to elucidate the effect of variation of **8A** on the lag phase and kinetics of growth. b) Gradual increase in size of assemblies with the concentration of **8A**. [**PN**] = [**MVCHO**] = 5×10^{-4} M, pH = 11.5.

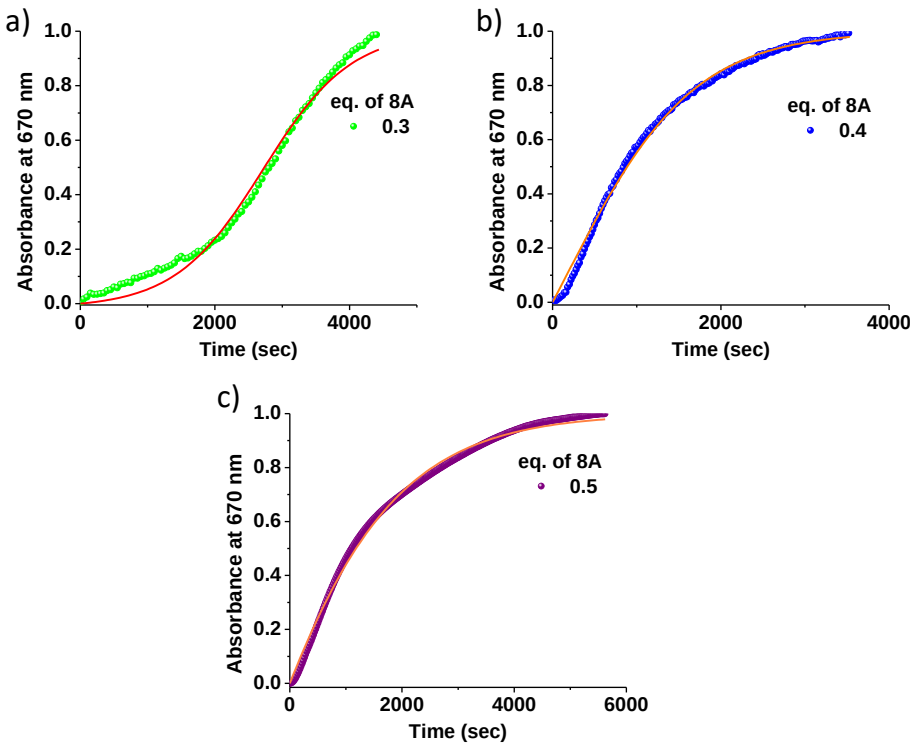

Figure S13. Finke-Watzky [S3] fit of temporal changes in absorption at 670 nm for calculating nucleation (k_n) and elongation (k_e) parameters on variation of **8A** corresponding to the experimental data in Figure 2d. [**8A**] = a) 0.3 eq., b) 0.4 eq. and c) 0.5 eq. [**PN**] = [**MVCHO**] = 5×10^{-4} M, pH = 11.5.

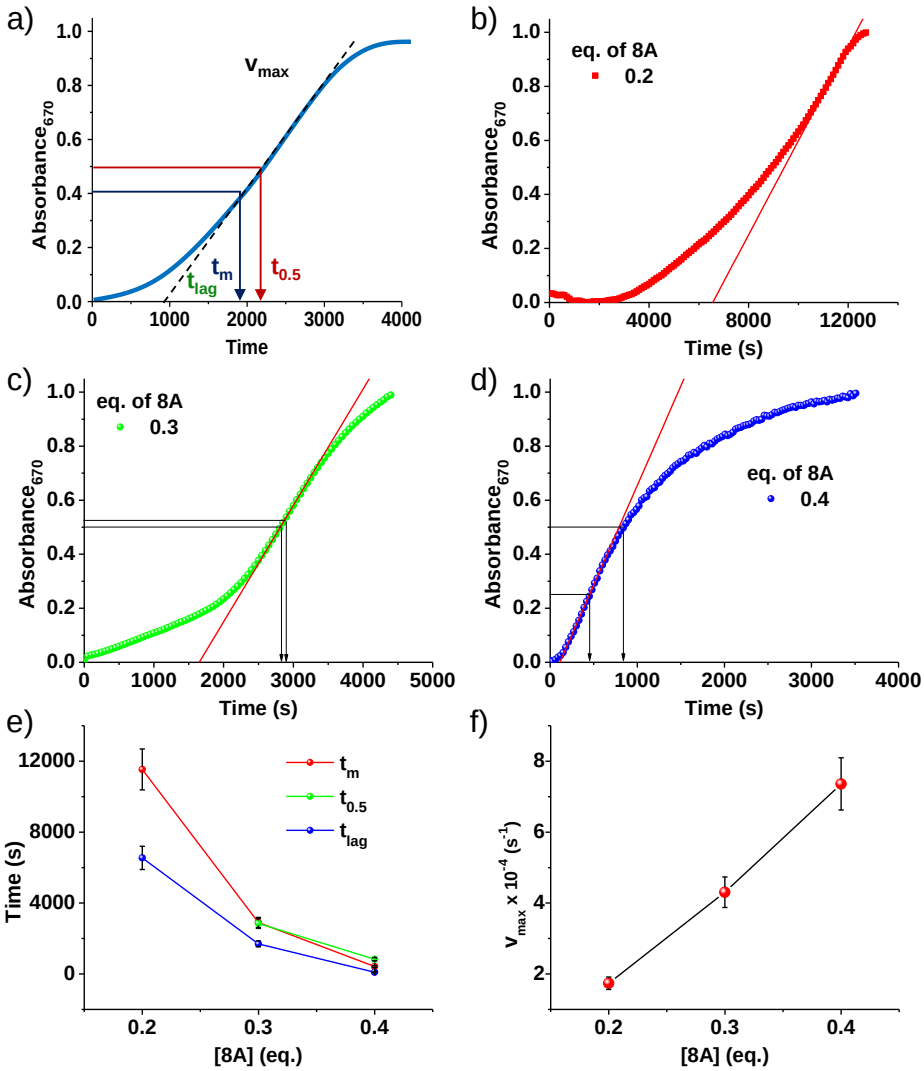

Figure S14. Fitting of absorption kinetics of unseeded supramolecular polymerization at different eq. of **8A** to obtain t_{lag}, $t_{0.5}$, t_m and v_{max}, a) Schematic representation. Calculation of kinetic parameters for b) 0.2 eq. **8A**, c) 0.3 eq. **8A**, d) 0.4 eq. **8A** and comparison of e) t_{lag}, $t_{0.5}$ and t_m and f) v_{max} and vs. eq. of **8A** corresponding to the experimental data in Figure 2d.

Note: To calculate the kinetic parameters, first order differential curve of kinetic profile was plotted vs. time. The peak maximum obtained is the t_m, i.e. time at maximum rate. In the kinetic trace a tangent is drawn around the maximum. The slope of tangent is the v_{max}, i.e. maximum rate. The tangent is extrapolated to y = 0. The time on the tangent line at y = 0 is the t_{lag} signifying the lag phase. The time when 50 % of growth has occurred is referred as $t_{0.5}$.

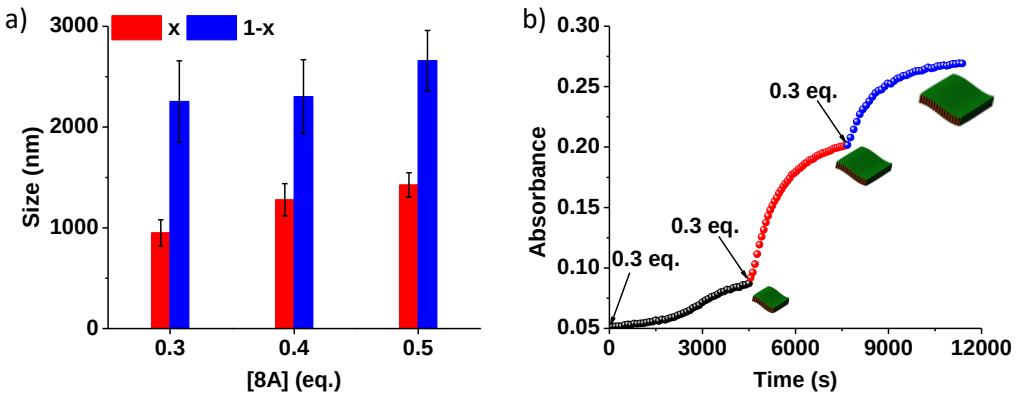

Figure S15. a) DLS size data for unseeded (x, red) and seeded (1-x, blue) assembly of **PN-MVCHO-8A**, where x represents the eq. of **8A** used to prepare seed solution (after unseeded kinetics). b) Temporal change in absorption at 670 nm for showing initial sigmoidal kinetics for unseeded growth with subsequent non-sigmoidal kinetics on seeding on addition of **8A** in three batches of 0.3 + 0.3 + 0.3 eq. **8A**. [**PN**] = [**MVCHO**] = $5x10^{-4}$ M, pH = 11.5.

Note: DLS has been only used as qualitative indicator and no quantitative analysis is drawn out of it.

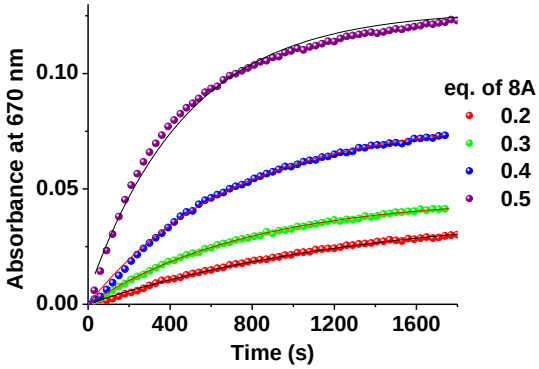

Figure S16. Fitting of seeded supramolecular polymerization curve to 1st order kinetics at different eq. of **8A** on seeding on 0.5 eq. **8A** seed. Absorption kinetics are monitored at 670 nm. [**PN**] = [**MVCHO**] = $5x10^{-4}$ M, pH = 11.5.

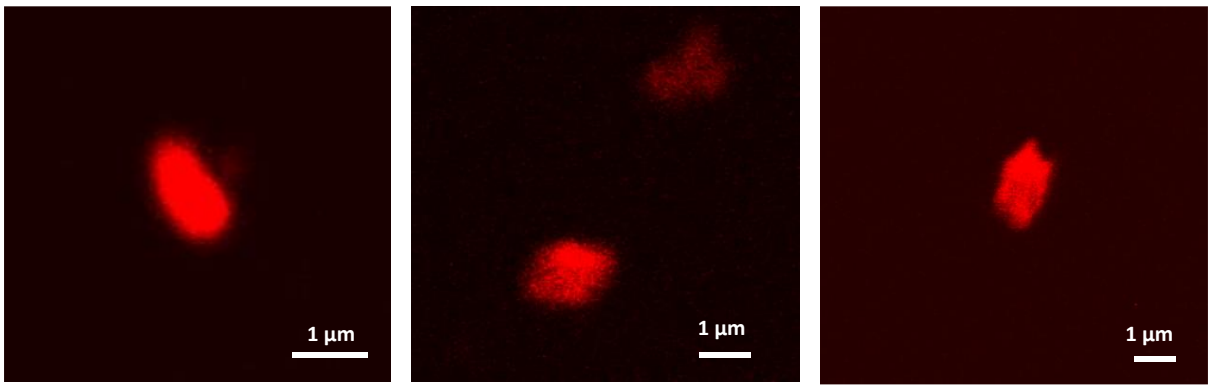

Figure S17. Confocal image (Nile red encapsulated in hydrophobic bilayer) of **PN-MVCHO-8A** assembly showing the formation of 2D sheets. [Nile red] = $1x10^{-6}$ M, [**PN**] = [**MVCHO**] = 5×10^{-4} M, [**8A**] = 0.5 eq., pH = 11.5.

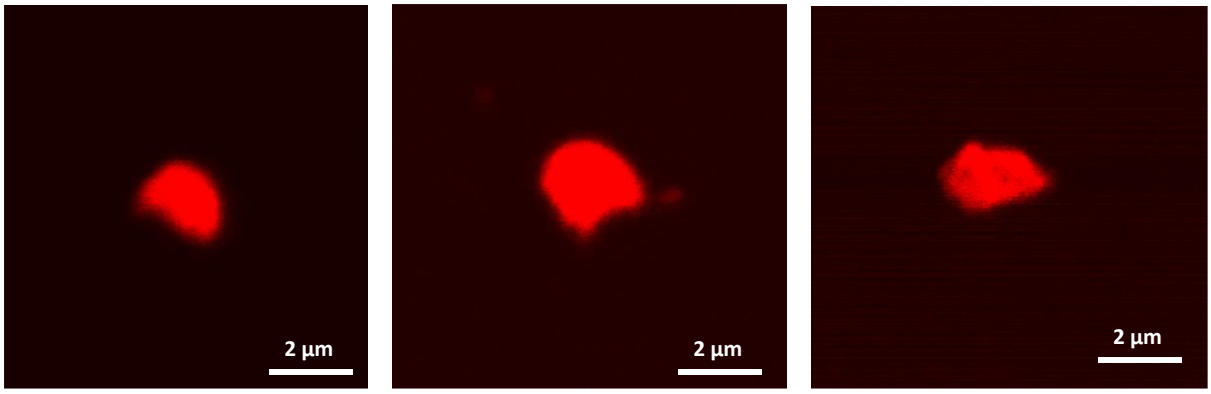

Figure S18. Confocal image (Nile red encapsulated in hydrophobic bilayer) of seeded **PN-MVCHO-8A** assembly showing the formation of 2D sheets. [Nile red] = $1x10^{-6}$ M, [**PN**] = [**MVCHO**] = 5×10^{-4} M, [**8A**] = 0.5 eq. (unseeded) + 0.5 eq. (seed), pH = 11.5.

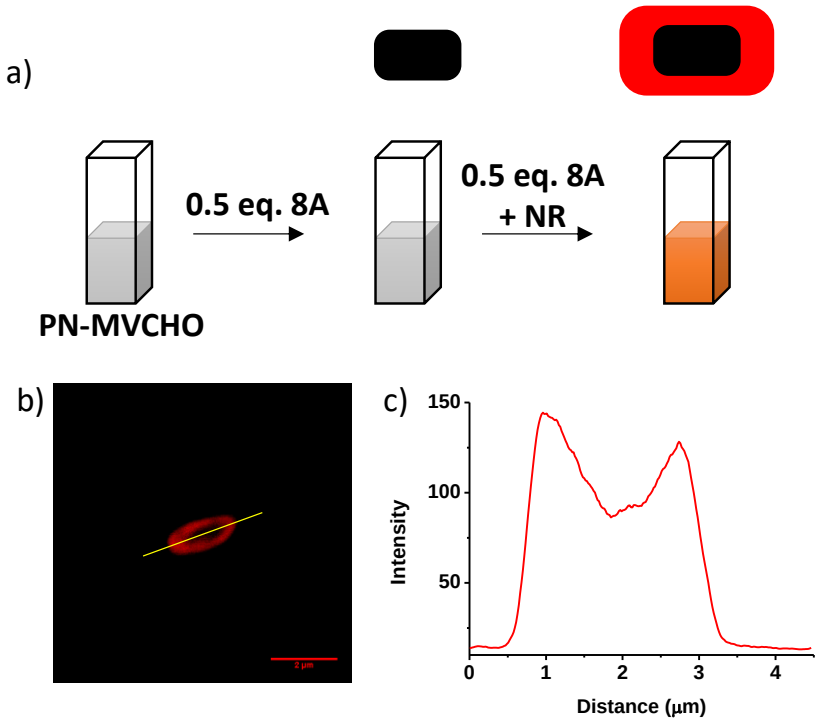

Figure S19. a) Schematic representation for the preparation method of sample for probing seeded supramolecular polymer. b) Confocal microscopy image showing a frame-like structure with dark (unseeded region) and fluorescent red (seeded region). c) Corresponding intensity profile of red emission with distance. [**PN**] = [**MVCHO**] = [**8A**] = 5×10^{-4} M, pH = 11.5, [Nile red] = 1 μM

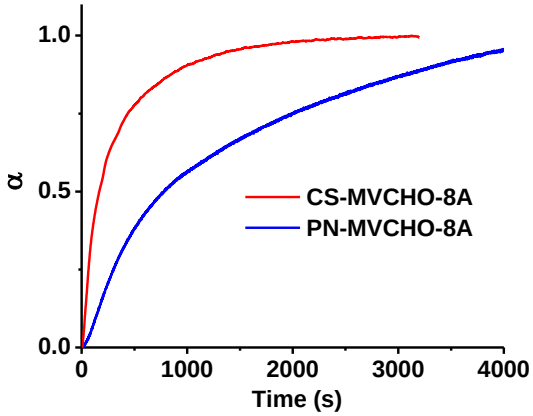

Figure S20. Kinetics of supramolecular polymerization of **8A** with **CS-MVCHO** and **PN-MVCHO**. [**CS**] = [**PN**] = [**MVCHO**] = [**8A**] = 5×10^{-4} M, pH = 11.5

Note: The comparison of the effect of supramolecular polymer on the kinetics of growth. As mentioned in the manuscript, the thermodynamic stability of the end product also affects the dynamic reaction equilibrium and an autocatalytic reaction occurs by the influence of thermodynamically driven supramolecular polymer. By keeping all experimental conditions same including the concentration and reactivity of amine, we compared the growth kinetics of **CS-MVCHO** and **PN-MVCHO**. The thermodynamic stability of end product influences the kinetics via autocatalysis. Thus, **CS-MVCHO-8A** with higher thermodynamic stability shows faster kinetics than **PN-MVCHO-8A**. In a single system, for example **PN-MVCHO-8A** the thermodynamic stability is same and hence the rate is determined by imine reaction i.e. concentration and reactivity.

6. References

S1. A. Jain, S. Dhiman, A. Dhayani, P. K. Vemula, S. J. George, *Nat. Commun.*, 2019, **10**, 450.

S2. C. Tanford, *J. Phys. Chem.*, 1972, **76**, 3020−3024.

S3. A. M. Morris, M. A. Watzky, R. G. Finke, *Biochim. Biophys. Acta* 2009, **1794**, 375-397.